Syn-Faulting Calcite Ages: Constraint for the Late Mesozoic Deformation of the Ningzhen Mountain, Eastern China

Jinbao Su ⓘ *[1], **Hongbing Tan**[2], **Yuexing Feng**[3], **Guoxing Qin**[2]

1. *College of Oceanography, Hohai University, Nanjing 210098, China*
2. *School of Earth Sciences and Engineering, Hohai University, Nanjing 210098, China*
3. *School of Earth Sciences, The University of Queensland, Brisbane QLD 4072, Australia*

ⓘ Jinbao Su: https://orcid.org/0000-0002-4354-3828

ABSTRACT: It is difficult to date a brittle fault because of the absence of effective dating methods. Recently, calcite U-Pb dating has drawn the attention of many researchers and has been successfully applied to constrain the age of brittle deformation. The South China Block (SCB) has experienced multiphase deformations characterized by widespread brittle faults and folds, which has led to significant debate on the Mesozoic dynamic mechanism and deformational phases. A syn-faulting calcite vein that occurred in the Permian limestones of the Ningzhen Mountain region was analyzed using U-Pb dating and geochemistry techniques in this paper. The U-Pb dating results display multiphase activities with two mixed ages of 109.9±5.8 Ma (MSWD=46, *n*=231) and 117.2±2.4 Ma (MSWD=3.6, *n*=150). The age of 117.2±2.4 Ma likely represents the timing of the brittle faults. Trace elements and rare earth elements data indicate that these fault-related calcites are mainly derived from host limestones and unrelated to Cretaceous magmatic activity. These faults formed in a tectonic reactive period and dormant time of the adakitic magma in the Lower Yangtze region.
KEY WORDS: U-Pb dating, calcite, South China Block, brittle fault, adakitic rock.

0 INTRODUCTION

The direct dating of faults is critical for reconstructing the deformation history of a continent. However, unlike the ductile shear zone, it is still a challenge to date brittle faults due to shallow-crust syn-tectonic minerals crystallizing in low-temperature conditions (Nuriel et al., 2011). Fault-fluid interactions have been discussed to understand fault mechanics and coseismic processes (Benedicto et al., 2008). A large number of fault-related fibers and veins were dated to constrain the fault activity using Sm-Nd and U-Th methods (Nuriel et al., 2011; Uysal et al., 2007a). These methods are valid in the case of having a large range of Sm-Nd ratios or limited time scales of 1–600 ka (Hansman et al., 2018). Similar drawbacks are also presented in apatite fission-track and (U-Th)/He dating (Su et al., 2017a; Spencer et al., 2006). The U-Pb dating of carbonates has been recently proved to have tremendous potential, for example, in dating calcite fibers of brittle faulting (Nuriel et al., 2017; Li Q et al., 2014; Rasbury and Cole, 2009; Benedicto et al., 2008).

Large-scale brittle faults have developed in the South

China Block (SCB) since the Mesozoic (Shu et al., 2015). Researches have been focused on the ductile deformation and magma activity of the SCB to constrain the regional tectonic events, which has led to a great deal of argument on their forming mechanism and detailed ages (Li J H et al., 2017; Chu and Lin, 2014; Su et al., 2014; Chu et al., 2012; Li and Li, 2007; Wang et al., 2005). The complex geological activities without ascertained timing also occurred in the Lower Yangtze region (LYR) of South China, where compression folding was superimposed by the Late Mesozoic–Cenozoic extension basin (Suo et al., 2019; Zhu et al., 1998). Furthermore, the Tan-Lu fault, its boundary, has maintained periodic activation since the Mesozoic (Zhu et al., 2004; Grimmer et al., 2002). As an arching orogen, the Ningzhen Mountain region has undergone all the above tectonic events and possesses adequate records in magmatism and faulting (Lu et al., 2019). However, it is still challenging to discriminate between these deformation periods, especially to distinguish the final building of E-W-trending orogen induced either by Indosinian or Yanshanian (Shu et al., 2015; Liu et al., 1992). Also, the influence of magmatism widely developed in the Ningzhen area on the formation of brittle faults is not clear.

Here, the fault-related calcites of Ningzhen Mountain were dated using the U-Pb method. Along with rare earth elements (REEs) and trace elements geochemistry, we discussed the source of the calcite precipitation and its relationship with the adjacent adakitic intrusive rocks. The direct dating of brittle
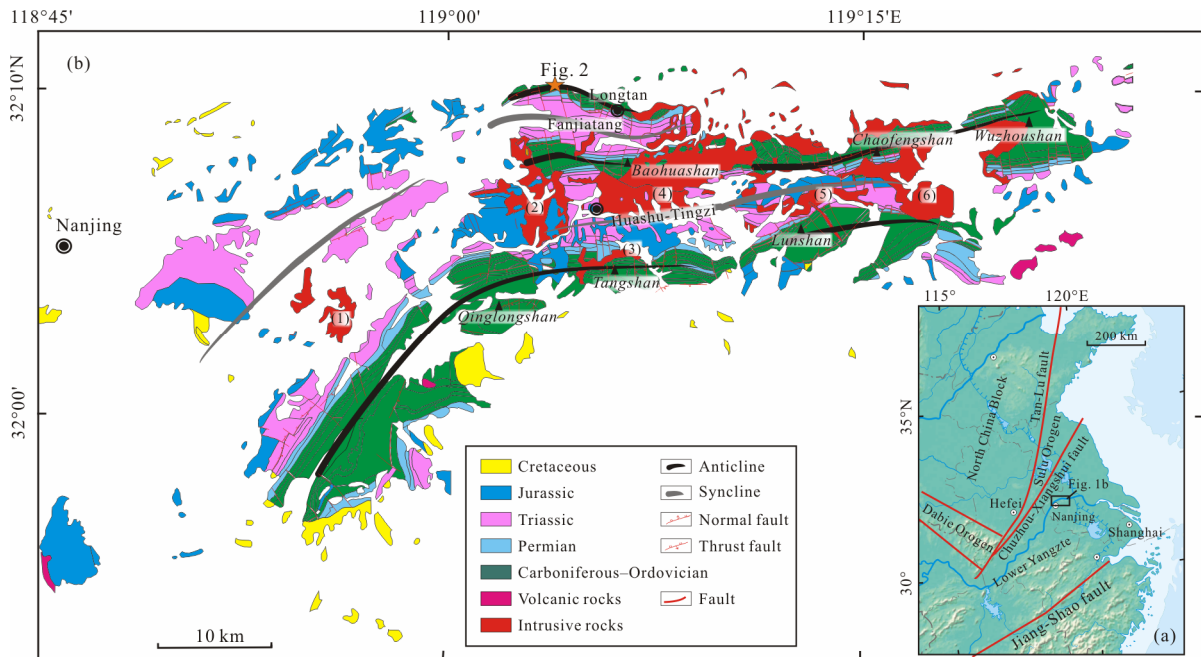
Figure 1. Sketch maps showing (a) the tectonic location of the study area and (b) the geological background of the Ningzhen Mountain region. Figure 1a modified after the topographic map of China (GS(2016)1609, http://bzdt.ch.mnr.gov.cn/). (1) Qilinmen pluton; (2) Anjishan pluton; (3) Funiushan pluton; (4) Xiaoshu-Gaozi pluton; (5) Xinqiao pluton; (6) Shima pluton.

faults in Ningzhen Mountain will highlight the further research of the Mesozoic deformation of South China.

1 GEOLOGICAL SETTING

The LYR is located in the northeast of SCB, in the eastern margin of the Yangtze Block (Fig. 1). It is separated from the Dabie-Sulu orogenic belt by the Tan-Lu and Chuzhou-Xiangshui faults to the west (Zhu et al., 2004; Liu et al., 2003; Gilder et al., 1999). The southern boundary of the LYR is the Jiang-Shao fault that formed a Neoproterozoic suture between the Yangtze and Cathaysia blocks (Li S Z et al., 2017; Su et al., 2017b). The LYR has a Meso–Neoproterozoic or older basement covered by a stable epicontinental deposition of clastic and carbonate rocks from the Nanhua period to the Middle Triassic (Chang et al., 2019; Su et al., 2018b; Xu et al., 2014). This depositional environment was broken by the following collision between the North and South China blocks in the Late Triassic (Kusky et al., 2007; Faure et al., 2001). As the foreland of Dabie-Sulu Orogen, the LYR was depressed during the Late Triassic–Middle Jurassic (Zhu et al., 1998). It was characterized by two unconformities where the Middle–Late Triassic Huangmaqing Group rested on and was overlain unconformably by the Early–Middle Triassic Qinglong Group and the Early–Middle Jurassic Xiangshan Group, respectively (Lu et al., 2019; Shu et al., 2008). Meanwhile, it shows bi-directional folding thrusts from the north and south toward the Yangtze River in this region (Xue, 2019; Zhu et al., 1998). Subsequently, the compressional environment continued to the Late Jurassic, while the Late Jurassic strata were either absent or unconformably overlain on the Xiangshan Group (Zhu et al., 1998). It's notable that more researchers considered the Middle–Late Jurassic compression event as a product of the subduction of the paleo-Pacific Plate (Lü et al., 2015; Li et al., 2012; Zhou et al., 2006). During the Cretaceous, magmatic activities occurred

widely, where igneous rocks intruded into Neoproterozoic low-grade metamorphic rocks and Paleozoic to Triassic sedimentary strata (Li et al., 2011).

Ningzhen Mountain trends nearly E-W with arching folds protruding north slightly (Fig. 1). It includes the Longtan-Cangtou, Baohuashan-Chaofengshan and Tangshan-Lunshan anticlines separated by the Fanjiatang and Huashu-Tingzi synclines, respectively, from north to south (Xue, 2019). The main faults are nearly E-W and N-S striking and conjugated faults trending NE and NW are also widely developed. Cretaceous intrusive rocks are mainly intermediate-acidic distributed along faults and in the cores of folds, including the Qilinmen, Anjishan, Xiashu-Gaozi, Shima and Xinqiao plutons (Fig. 1) (Li et al., 2011; Xu et al., 2002).

2 SAMPLING AND ANALYTICAL METHODS
2.1 Sampling

The strata in the Ningzhen Mountain region has been folded, where the Permian limestone strata developed into a monoclinic structure dipping south at Longtan (Fig. 2). Fault planes and calcite-filled veins were measured and documented in the field. In this outcrop profile, a near N-S-trending fault (Figs. 2b and 2h) and near E-W-trending fault developed (Figs. 2a and 2c–2g). There is no obvious crosscut relationship between these two trending faults (Fig. 2). These faults dip 50°–60° with simple kinematic geometry and nearly parallel to the attitude of the strata (Fig. 2i). The near E-W-trending faults illustrate more thrust and strike-slip information. For example, the calcite vein BH519-11 has been cut with a small thrust-fault throw (Fig. 2d); a fault-related rhombic lens and slip striations indicate a thrust fault direction (Figs. 2e and 2f); and the calcite veins were thrust forming a drag fold (Fig. 2g). A total of 21 samples (location: 32°9'35"N, 119°4'49"E) were collected from
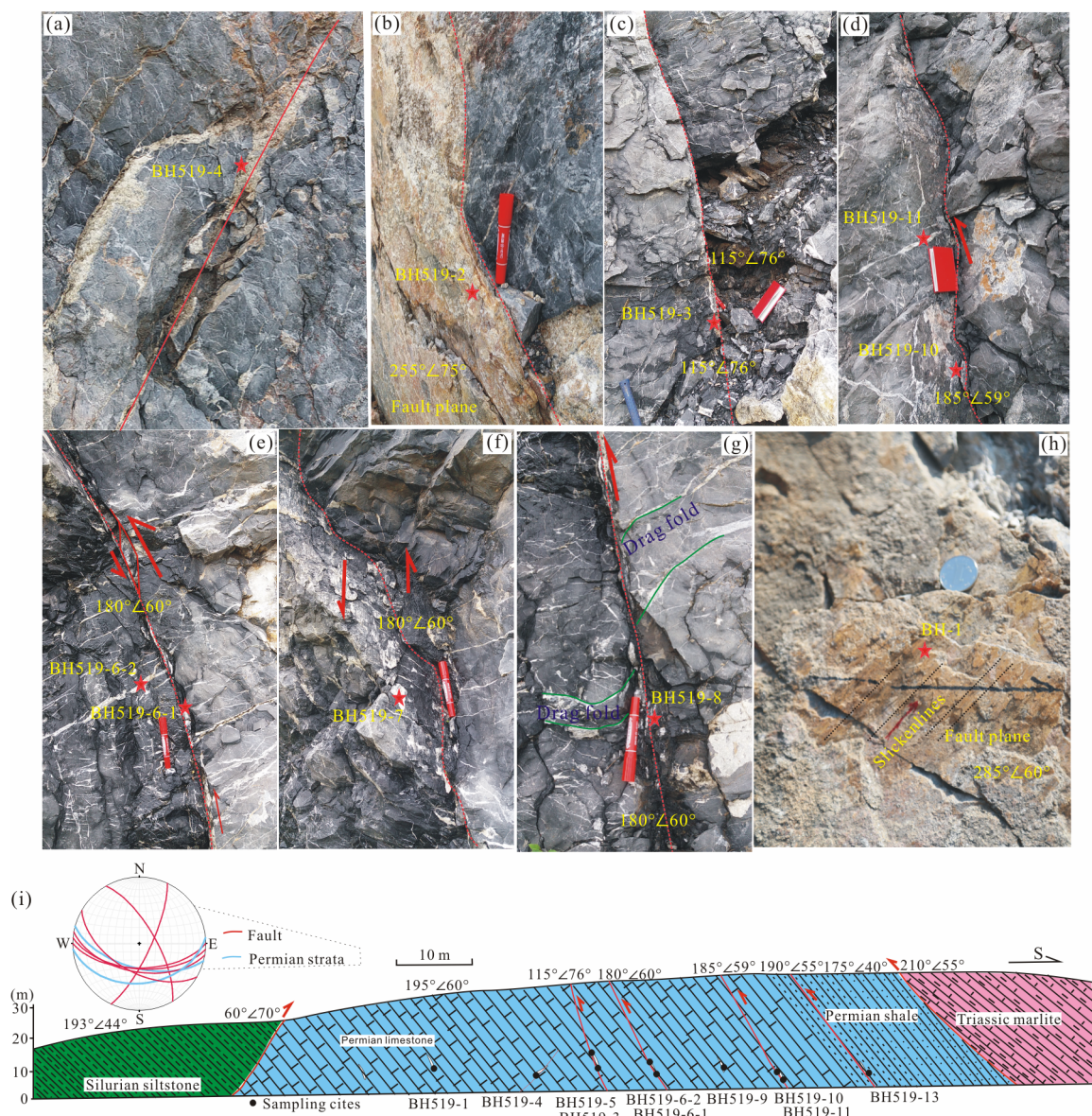
Figure 2. Field photographs showing (a)–(h) the representative brittle faults and calcite vein samples; and (i) a geological profile showing the sampling outcrop and stereographic projection of main faults.

the above fault-related calcite veins, slip striations and host rocks along with the structure profile (Fig. 2). The slip striations are syn-tectonic with faults. Meanwhile, the faults cut some calcite veins. These slip striations and cutting calcite veins were collected to constrain the fault age. Samples are described in Table 1.

2.2 Analytical Methods

The concentrations of trace elements and REEs were determined using the pressurized acid digestion method of Guizhou Tongwei Analytical Technology Co., Ltd. The resulting solutions were analyzed by inductively coupled mass spectrometry (ICP-MS). The methods, detection limits, and instrument conditions are described by Lawrence and Kamber (2006). The international standard materials W-2a, BHVO-2, and JCP-1 were analyzed to calibrate the calcite samples for quality control.

The U-Pb dating was carried out using a Nu plasma multi-collector inductively-coupled plasma mass spectrometer (MC-

ICP-MS) coupled to an excimer laser ablation system in the Radiogenic Isotope Facility at the School of Earth Sciences, The University of Queensland. Faraday cups and ion-counting secondary-electron multipliers with off-line gain calibration were used for detection. The spot size of ablation was 100 μm with a dwell time of 21 s. The U and Pb concentrations were tested semi-quantitatively against reference AHX. The ^{207}Pb/^{206}Pb ratios were mass-bias corrected using NIST614 for the accepted Pb isotope composition. A similar method has been applied and described in other studies (Li Q et al., 2014).

3 RESULTS
3.1 Trace Elements and REEs

The concentrations of trace elements and REEs of the host rocks and calcite vein samples are presented in Table 2. Primitive mantle-normalized trace element and chondrite-normalized REE patterns of the samples are shown in Fig. 3. In general, the calcite samples are similar in spidergram patterns. They are

Table 1 General description of fault-related calcite and host rock samples

Samples	Lithology	U/Pb	Sm/Nd	Mg/Ca	Mn/Fe	Sample location	Structure strike
BH-1	Calcite	0.000	0.152	0.002	0.436	Fault plane	195°
BH-2	Calcite	0.004	0.195	0.002	0.377	Vein	
BH-4	Calcite	0.005	0.235	0.002	0.378	Vein	
BH519-1	Calcite	1.216	0.260	0.003	0.511	Fault plane	165°
BH519-2-1	Calcite	0.512	0.258	0.003	0.436	Fault plane	165°
BH519-2-2	Calcite	0.124	0.251	0.002	0.377	Fault plane	165°
BH519-3-1	Calcite	0.532	0.226	0.004	0.195	Fault plane	205°
BH519-4	Calcite	0.263	0.243	0.001	0.109	Fault plane	
BH519-5	Calcite	0.000	0.201	0.002	0.205	Vein	
BH519-6-1	Calcite	1.308	0.241	0.005	0.109	Fault plane	90°
BH519-6-2	Calcite	0.443	0.211	0.007	0.065	Vein	
BH519-7	Calcite	0.136	0.268	0.005	0.108	Fault plane	90°
BH519-8	Calcite	0.083	0.293	0.004	0.173	Fault plane	90°
BH519-9	Calcite	0.002	0.212	0.004	0.065	Fault plane	225°
BH519-10	Calcite	2.984	0.176	0.004	0.121	Fault plane	95°
BH519-11	Calcite	2.664	0.203	0.008	0.067	Vein	
BH519-13	Calcite	1.372	0.255	0.005	0.024	Fault plane	95°
BH519-1S	Limestone	0.213	0.195	0.009	0.225	Host rock	80°
BH519-11S	Limestone	0.171	0.194	0.007	0.163	Host rock	80°
BH-1S	Limestone	0.096	0.134	0.243	0.066	Host rock	80°
BH519-8S	Limestone	0.327	0.216	0.010	0.050	Host rock	80°

enriched in trace elements U and Sr and depleted in Ta, Nb, Zr, Hf, and Ti. In contrast, the host rocks can be differentiated from the calcite samples due to their lower degree of depletion in the above corresponding elements. An inconsistency is seen for element Ba, which shows a positive anomaly in most calcites and negative anomaly in host rocks. The concentrations of REEs are slightly higher in host rocks than in most of the calcite samples, however, their spidergrams are not easily distinguishable. These samples illustrate higher light REEs than heavy REEs and exhibit a negative Eu anomaly.

3.2 U-Pb Ages

The concentrations in the 17 calcite veins obtained by ICP-MS vary from 0.016 9 ppm to 18.6 ppm for U and from 0.014 8 ppm to 648 ppm for Pb. Low concentrations of U and radiogenic Pb (low U-Pb ratios) of carbonates are unsuitable for dating by either isotope dilution or laser ablation approaches (Li Q et al., 2014). Therefore, only two samples were dated and their U-Pb ages were acquired. The analytical results were plotted in concordia diagrams (Fig. 4), where the ages were calculated as lower isochron intercepts using Isoplot 3.0 (Ludwig, 2003); these are 117.2±2.4 Ma (MSWD=3.6, n=150) for sample BH519-10 and 109.9±5.8 Ma (MSWD=46, n=231) for sample BH519-11 (the U-Pb analyses data see Table S1).

4 DISCUSSION
4.1 Age and Geochemistry

The carbonate diagenetic system is difficult to date due to an unclear initial isotopic composition and varied U/Pb in dif-

ferent minerals formed at the same time. Fluid flow also alters minerals or creates secondary precipitates changing the primary deposit (Rasbury and Cole, 2009). This implies the existence of likely scattered U/Pb isotopic data with large mean squared weighted deviates (MSWD). Similar results are present in other research (Hansman et al., 2018). The age 117.2±2.4 Ma for sample BH519-10 has MSWD=3.6, attributable to an underestimated analytical error due to 150 analysis spots. We cannot completely exclude the influence of variations of ages within a calcite vein. The research region underwent multiphase tectonic events (Zhu et al., 1998), which may have led to polyphasic vein cement. Sample BH519-11 is an excellent example of this, with an age close to that of sample BH519-10. However, it is unconcordant for the age of 109.9±5.8 Ma with MSWD=46 (n=231), representing an inaccurate mixed age of the calcite vein (Fig. 4b). Indeed, the sample BH519-11 is located in a near-horizontal vein, whereas sample BH519-10 is a vein located in a fault that cut the BH519-11 with a small fault throw (Fig. 2d). Such a close location and age give us reason to believe that the age of 117.2±2.4 Ma (sample BH519-10) constrains the forming time of the brittle fault and the horizontal vein (Sample BH510-11) correlates significantly with the fault. The geochemistry of both samples shows a consistent pattern in trace elements and REEs further indicating their inherent connection (Fig. 3).

The collected samples are from veins located on the planes of the near S-N-strike and E-W-strike faults (Fig. 2). Unfortunately, no other dated data was obtained due to the low concentrations of U and Pb of the samples. During different calcite

Table 2 Elemental concentration (ppm) of the fault-related calcite veins and host rocks of the Ningzhen Mountain

Samples	BH-1	BH-2	BH-4	BH519-1	BH519-2-1	BH519-2-2	BH519-3-1	BH519-4	BH519-5	BH519-6-1
Li	0.042 6	0.034 8	0.03 6	0.025 8	0.027 9	0.026 2	0.141	0.077 6	0.027 7	0.142
Be	0.004 08	0.038 1	0.016 7	0.036 1	0.049 4	0.045 3	0.092	0.019 9	0.014 7	0.034
Mg	809	808	851	1 530	1 190	1 020	1 950	523	981	2 060
P	32.1	41.2	32.7	52.5	56	57.7	38.7	35.2	37.3	28.7
Ca	442 000	444 000	452 000	443 000	445 000	439 000	443 000	446 000	447 000	444 000
Sc	0.173	0.225	0.2	0.455	0.34	0.232	0.186	0.157	0.155	0.14
Ti	0.138	0.118	0.484	0.074 7	0.12	0.088 5	0.112	0.084 6	0.042 6	0.003 88
V	2.37	16.9	0.181	25	18.7	10.9	7.95	8	nd	3.84
Fe	2 290	3 370	1 950	4 600	4 410	2 970	1 860	2 780	1 840	1 850
Co	1.75	1.01	1.13	1.57	0.917	1.12	0.6	0.664	1.83	0.613
Ni	11.8	8.9	9.98	7.7	7.56	9.62	6.63	6.88	11.3	6.69
Cu	0.672	0.731	1.06	0.743	0.882	1.14	0.695	0.995	0.79	0.688
Zn	313	254	64.1	27.1	43.6	118	1.47	4.46	131	1.34
Ga	0.030 7	0.043 3	0.046 4	0.112	0.097	0.051 6	0.024 1	0.016 8	0.017 2	0.014 7
Rb	0.038 2	0.053 5	0.043 9	0.029 3	0.062 6	0.042 9	0.024 4	0.035 6	0.020 1	0.031 5
Sr	59.1	122	74.9	200	139	87.2	490	220	75.9	1 020
Y	0.527	1.36	2.52	12.9	12.1	3.07	1.27	0.811	0.454	0.854
Zr	0.709	0.767	0.152	0.055 5	0.088 7	0.183	0.094 1	0.014 7	0.117	0.014 7
Nb	0.002 74	0.002 62	0.003 13	0.001 65	0.001 65	0.001 71	0.001 84	0.001 91	0.002 66	0.002 54
Mo	0.002 17	0.004 22	0.107	0.043 1	0.226	0.117	0.009 2	0.085 4	0.025 9	0.009 68
U	0.016 9	1.41	0.234	18.6	12.6	7.35	0.665	1.12	0.017	0.654
Sb	0.001 87	0.033 8	0.029 3	0.135	0.147	0.105	0.003 98	0.077 6	0.012 2	0.004 63
Cs	0.001 24	0.002 02	0.007 52	0.000 636	0.002 02	0.002 72	0.003 84	0.008 52	0.000 85	0.006 85
Ba	0.136	1.16	0.1	87.8	311	573	3.96	1.2	0.203	5
La	0.225	0.607	1.04	4.24	3.94	1.08	0.705	0.366	0.185	0.414
Ce	0.486	1.19	2.37	7.63	6.61	1.72	1.43	0.962	0.336	0.971
Pr	0.067 8	0.152	0.32	0.912	0.791	0.229	0.175	0.134	0.039 1	0.127
Nd	0.309	0.661	1.37	3.77	3.39	0.961	0.727	0.567	0.163	0.519
Sm	0.046 9	0.129	0.322	0.979	0.873	0.241	0.164	0.138	0.032 7	0.125
Eu	0.009 45	0.028	0.079 5	0.314	0.29	0.084 3	0.032 3	0.026 9	0.008 42	0.011 2
Gd	0.043 4	0.137	0.358	1.49	1.35	0.338	0.176	0.127	0.039 5	0.127
Tb	0.006 42	0.021 3	0.056 4	0.252	0.221	0.055 9	0.025 9	0.019 9	0.007 36	0.020 2
Dy	0.037 7	0.134	0.299	1.52	1.36	0.325	0.143	0.113	0.041 9	0.12
Ho	0.009 06	0.029 2	0.059 2	0.299	0.282	0.068 1	0.030 6	0.022 2	0.008 86	0.023 5
Er	0.026 8	0.084	0.165	0.786	0.725	0.177	0.078 7	0.057 8	0.026 7	0.060 9
Tm	0.003 77	0.012 6	0.023 4	0.105	0.096 4	0.023 1	0.011	0.008 59	0.003 99	0.008 7
Yb	0.023 2	0.074 8	0.139	0.58	0.535	0.133	0.063 6	0.052 8	0.022 5	0.046 7
Lu	0.004 04	0.012	0.022 4	0.082 3	0.075 2	0.018 4	0.008 44	0.008 08	0.003 5	0.006 9
Hf	0.006 47	0.006 18	0.001 68	0.001 19	0.001 94	0.001 77	0.002 69	0.000 003	0.000 908	0.000 137
Ta	0.000 386	0.000 241	0.000 387	0.000 32	0.000 387	0.000 29	0.000 318	0.000 267	0.000 207	0.000 251
Pb	648	385	49.1	15.3	24.6	59.3	1.25	4.26	59.7	0.5
Th	0.004 71	0.020 5	0.007 78	0.012 9	0.009 77	0.005 86	0.007 57	0.016 3	0.003 81	0.037 4

Table 2 Continued

| Samples	BH519-6-2	BH519-7	BH519-8	BH519-9	BH519-10	BH519-11	BH519-13	BH519-1S	BH519-11S	BH-1S	BH519-8S
Li	0.099 6	0.094 2	0.023 8	0.054 6	0.141	0.103	0.080 6	3.4	0.794	2.13	6.2
Be	0.19	0.024 7	0.091 6	0.138	0.020 9	0.005 76	0.001 44	0.249	0.109	0.384	0.555
Mg	2 930	2 200	1 750	1 760	1 810	3 570	2 180	3 550	2 920	63 700	4 060
P	30.8	37.4	47.6	101	24.4	21.6	24.3	257	11.6	214	22.4
Ca	448 000	435 000	445 000	453 000	443 000	440 000	434 000	385 000	401 000	262 000	391 000
Sc	0.151	0.153	0.207	0.304	0.148	0.134	0.129	1.41	0.749	1.82	2.11
Ti	0.125	0.173	0.106	0.237	0.077 1	0.213	0.075	199	46.8	661	363
V	1.36	6.45	2.44	nd	5.66	1.85	0.029 6	24.2	5.15	72	38.9
Fe	2 340	4 570	5 170	1 870	1 790	1 770	1 740	3 600	836	14 700	3 740
Co	0.592	0.606	0.934	0.698	0.609	0.601	0.587	7.66	0.75	4.08	1.04
Ni	6.28	6.68	9.87	13.6	6.78	6.51	5.88	25.8	2.28	37.5	11
Cu	2.17	0.703	0.773	1.4	0.721	0.689	2.11	6.07	0.609	13	3.31
Zn	4.63	1.06	16	516	1.44	0.989	1.83	83.5	34	114	26.4
Ga	0.026 6	0.019 8	0.045 1	0.02	0.015 3	0.014 2	0.008 67	1.24	0.253	2.36	3.8
Rb	0.124	0.072 9	0.038 2	0.055 1	0.05	0.040 8	0.024 5	7.56	1.74	17.3	25.7
Sr	2 510	3 180	225	63.3	824	2 160	856	1 320	812	642	2 520
Y	1.37	0.794	4.41	1.11	0.35	0.711	2.66	2.79	0.696	2.39	9.72
Zr	0.032 9	0.005 28	0.013 4	0.296	0.014 9	0.005 1	0.001 23	10.3	1.5	25	36.5
Nb	0.001 21	0.002 16	0.001 12	0.001 8	0.002 3	0.002 02	0.001 48	0.91	0.199	2.85	3.55
Mo	0.023 9	0.054	0.012 9	0.024 6	0.016 7	0.008 06	0.003 82	0.287	0.070 1	0.593	0.455
U	0.593	0.374	4.06	0.143	0.955	0.714	0.020 3	3.64	1.61	5.63	4.45
Sb	0.473	0.009 16	0.001 59	0.018 6	0.008 82	0.007 42	0.001 47	0.517	0.104	2.9	0.757
Cs	0.008 67	0.004 78	0.000 461	0.005 43	0.007 8	0.003 51	0.002 12	0.809	0.098 4	2.62	1.7
Ba	9.53	5.01	0.107	0.812	4.25	2.68	5 560	173	6.2	26.6	98.1
La	1.05	0.204	1.13	1.03	0.245	0.483	1.07	3.08	0.694	7.05	10.3
Ce	2.24	0.54	2.67	2.26	0.571	1.06	1.01	5.88	1.36	10.6	21.6
Pr	0.265	0.074 1	0.367	0.287	0.074 1	0.126	0.152	0.692	0.165	1.01	2.5
Nd	1.04	0.33	1.63	1.12	0.294	0.487	0.599	2.63	0.638	3.17	9.39
Sm	0.219	0.088 4	0.478	0.237	0.051 6	0.099	0.153	0.513	0.124	0.425	2.03
Eu	0.053	0.013 2	0.1	0.053 1	0.009 7	0.019 9	0.093	0.102	0.025 5	0.070 5	0.131
Gd	0.219	0.108	0.671	0.213	0.042 9	0.095 8	0.193	0.532	0.126	0.521	2.03
Tb	0.034 1	0.016 9	0.111	0.030 8	0.005 35	0.012 3	0.032 4	0.073 4	0.017 4	0.063	0.311
Dy	0.193	0.101	0.604	0.163	0.034 9	0.072	0.221	0.397	0.095 3	0.345	1.73
Ho	0.039 1	0.020 1	0.116	0.029 9	0.006 83	0.013 8	0.054 2	0.081 1	0.019 5	0.074 6	0.349
Er	0.102	0.050 3	0.29	0.081 1	0.018 4	0.036 6	0.165	0.225	0.051 7	0.226	0.988
Tm	0.014 2	0.007 46	0.040 2	0.011 4	0.002 64	0.004 91	0.023 8	0.033 8	0.007 93	0.037 7	0.151
Yb	0.084 5	0.041 9	0.235	0.073 1	0.017 9	0.023	0.139	0.209	0.046 1	0.252	0.973
Lu	0.012 8	0.006 32	0.035 2	0.011 2	0.002 64	0.003 76	0.020 5	0.033	0.007 17	0.040 7	0.15
Hf	0.000 625	0.000 202	0.000 524	0.002 38	0.000 201	0.000 22	0.000 592	0.27	0.039 8	0.634	1.28
Ta	0.000 231	0.000 302	0.000 319	0.000 203	0.000 213	0.000 14	0.000 091 1	0.077 1	0.022 1	0.169	0.267
Pb	1.34	2.74	48.7	58.9	0.32	0.268	0.014 8	17.1	9.4	58.9	13.6
Th	0.136	0.034 5	0.033 6	0.012 8	0.007 16	0.005 02	0.001 92	0.815	0.115	1.56	3.22
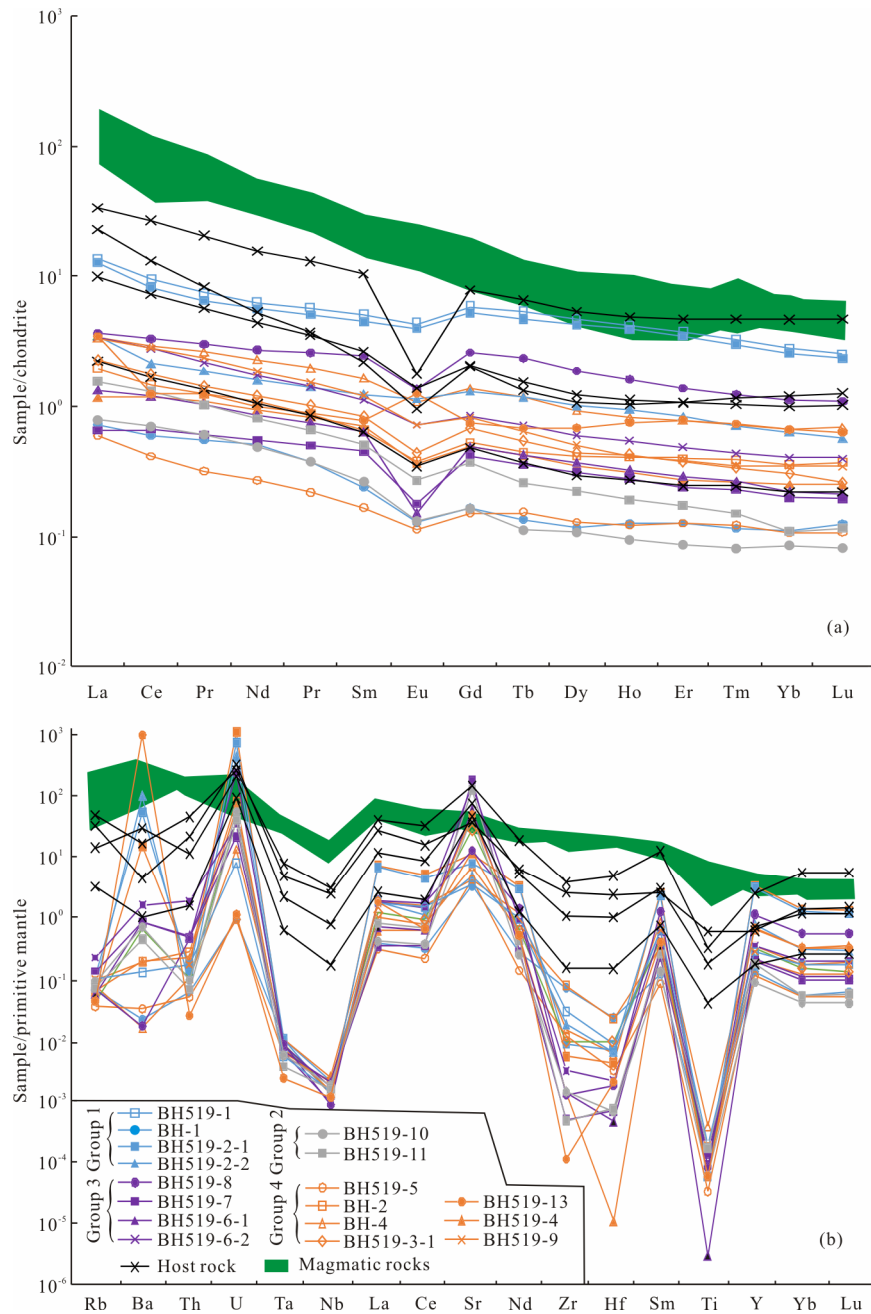
Figure 3. Spidergrams for chondrite-normalized REEs and primitive mantle-normalized trace elements. Group 1. calcite veins in near S-N-striking fault; Group 2. calcite samples in the same fault (see location in Fig. 2); Group 3. calcite samples in another fault (see locations in Fig. 2); and Group 4. calcite samples in near E-W-striking faults; host rock. Permian carbonate rocks; magmatic rocks. adakitic intrusive rocks exposed in the Ningzhen region (Lu et al., 2019).

generations, the differences in REE compositions can be attributed to variations in the water-rock interaction processes (Uysal et al., 2007b). As shown in Fig. 3, all the calcite samples have similar REE patterns except for samples BH519-1 and BH519-2-1, which have little high concentrations and are closer to the host carbonate rocks. The other samples (BH519-2-2 and BH-1) collected from the same fault plane (near S-N strike) have similar REE contents as the samples located in the near E-W-striking faults. Geochemistry differentiation is difficult for these calcite veins, implying that they may have the same source. In contrast, unlike the source of the calcite veins even despite their occurrence at similar times, the Late Cretaceous magmatic rocks that intruded in the Ningzhen

region show different trace elements and REEs patterns (Fig. 3) and are unlike the source of the calcite veins even despite their occurrence at similar times. Undoubtedly, the host carbonate rocks provide the main source of the calcite vein, however, the difficulty in ascertaining the periods of tectonic activities increases due to similar geochemistry characters.

4.2 Tectonic Implications

The fold-thrust structural belt of South China was considered being formed in the Mesozoic based on the contact relationship of the faults and folded strata. Widespread fault activities have no detailed timing due to their brittle property. It is hard to distinguish these kinds of faults from the Mesozoic
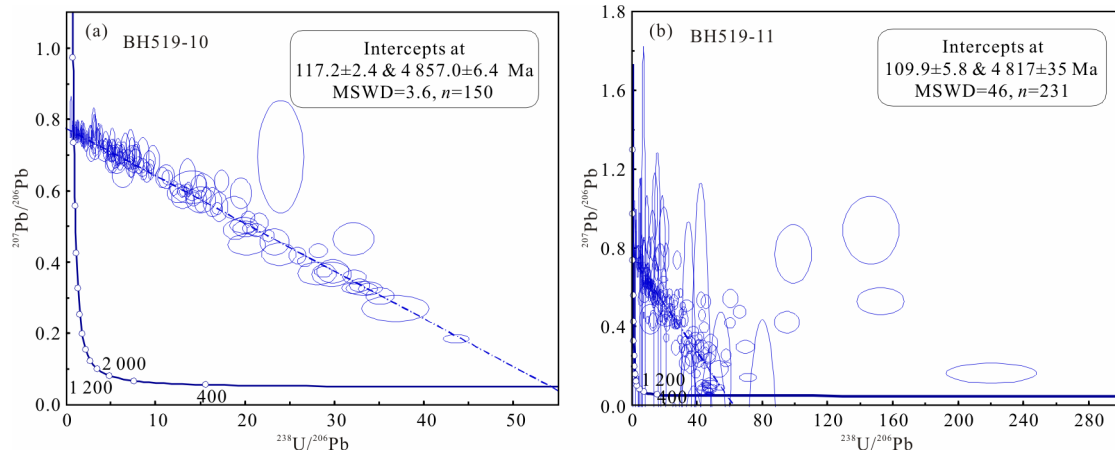
Figure 4. Concordia diagrams showing the U-Pb ages of fault-related calcite veins. (a) Sample BH519-10; (b) Sample BH519-11.

Indosinian or Yanshanian orogeny in the absence of a corresponding relationship among strata in the SCB. Many researchers analyzed the fault-slip information of South China to restore its paleo-stress, and then ascertain different tectonic activities together with regional magmatic events (Li et al., 2016; Su et al., 2013). However, the mistakes were unavoidable due to uncertain ages. In fact, it is difficult to exclude the younger tectonic activity consistent with a regional structural framework. The structures of LYR are mainly trending ENE-NE, E-W and NW-NWW, forming an arch protruding north in the Ningzhen region. Zhu et al. (1998) proposed that the LYR was a near E-W-trending fold belt during Late Triassic–Middle Jurassic and was transformed into the present ENE-NE-trending structure due to the strike-slip effect of Tan-Lu fault. The near E-W-trending Ningzhen Mountain could be the product of transpression in the Late Jurassic (Chang et al., 2019). Anyway, Ningzhen Mountain inherited its own nappe structure after multiphase tectonic events (Liu et al., 1992; Ge, 1987). Obviously, it is not precise that the large scale of brittle faults and cleavages developed in the Ningzhen region were attributed to Indosinian or Yanshnian orogeny (Li et al., 2018). The age of fault-related calcite veins in this work defines a new tectonic event that occurred in 117–109 Ma in the Ningzhen Mountain. The dated fault is a thrust fault according to the motion character of elongate lenses and sliding steps, indicating a compressive event (Fig. 2). This age is consistent with the dormant time of 117–108 Ma for the magmatic activity, which is considered a tectonic inversion stage in South China (Li J H et al., 2014). It gave rise to NW-SE-direction compression associated with widespread folding, strike-slip faulting and sinistral ductile shearing along the coastal Changle-Nan'ao fault zone (Shu et al., 2009; Lapierre et al., 1997; Charvet et al., 1994). The brittle faults in the study area generally parallel to or perpendicular to the structural strike of the Ningzhen Mountain and probably have not escaped the influence of the early structure.

Notably, a large amount of Early Cretaceous adakitic intrusive rocks are exposed in the Ningzhen region (Lu et al., 2019; Ling et al., 2009). Researchers proposed that the crustal thickness of the LYR exceeded 40 km in the Early Cretaceous and then began thinning due to lower-crustal delamination (Xu et al., 2002). Ling et al. (2009) argued against the Mesozoic crustal thickening in the region because it is not supported by

the development of extensional basins. The adakitic rocks intruding in the Ningzhen region are distributed in a nearly E-W trending in plain view and are 10–30 Ma later than those in the other LYR regions (Xue, 2019). The fault calcites in our paper only occurred in this magmatically dormant period. Although controlled by the same Pacific Plate, eastern China experienced polyphase transformations of tectonic stress fields during the Cretaceous (Zhang et al., 2003). Considering Cretaceous tectonic stress, magmatic activity, and paleogeography, the fault calcites of the Ningzhen Mountain may record the above transition in magmatic and tectonic events. The effects of asthenospheric mantle uplifting and stress relaxation of compression orogeny led to lithospheric thinning of the LYR from 140 to 120 Ma (Fig. 5a). During this time, the Tan-Lu fault might have been a dextral transcurrent fault that accommodated NW-SE crustal extension and magmatic intrusion in the LYR (Zhang et al., 2003); however, it has little effect on the Ningzhen region. Subsequently, the collision of the West Philippine Block with the eastern Asian margin (Zhang et al., 2019; Faure et al., 1989) and the roll-back of the subduction plate induced a short-time compression against the east of the Chinese continent (Su et al., 2018a; Zhou et al., 2006). The Tan-Lu fault appeared as sinistral transpression and produced an S-N-direction compression in the region (Zhu et al., 2018). It likely resulted in some brittle deformation of the upper crust associated with fault-related calcite veins and tectonic inversion from 120 to 110 Ma (Fig. 5b). Meanwhile, the brittle faults probably inherited the pre-tectonic deformation, leading to mixed U-Pb ages (Fig. 4) and E-W-trending faults in the Ningzhen region. After the short dormancy, the adakitic magma began to be active in Ningzhen and its eastern region due to lithospheric delamination induced by the sustained subduction of the Pacific Plate (Xu et al., 2002) (Fig. 5c). The regional stress regime manifested S-N-direction extension associated with local rift basins (Zhu et al., 2018).

5 CONCLUSION

The fault-related calcites of the Permian carbonate in Ningzhen Mountain yield U-Pb ages of 117.2±2.4 and 109.9±5.8 Ma, which constrain the timing of brittle fault activity. The trace elements and REEs indicate that the fault-related calcites were mainly derived from the host carbonate rocks rather than the
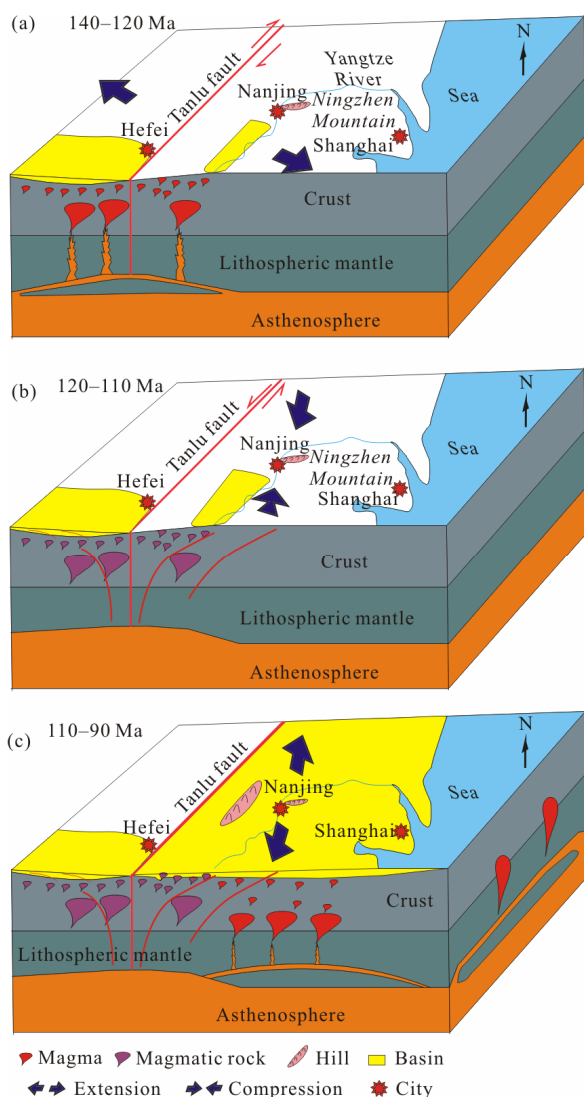
Figure 5. Cartoons showing the tectonic evolution of the LYR and stress regime in the Ningzhen area. (a) Adakitic magma intrusion in the LYR of 140–120 Ma; (b) forming time of fault-related calcite veins in Ningzhen Mountain of 120–110 Ma; and (c) adakitic magma occurring in Ningzhen Mountain of 110–90 Ma.

magmatic rocks. The analyzed brittle faults occurred likely as the product of short-time tectonic inversion during the dormant period of magmatic activity.

REFERENCES CITED

Benedicto, A., Plagnes, V., Vergély, P., et al., 2008. Fault and Fluid Interaction in a Rifted Margin: Integrated Study of Calcite-Sealed Fault-Related Structures (Southern Corinth Margin). *Geological Society, London, Special Publications*, 299(1): 257–275. https://doi.org/10.1144/sp299.16

Chang, Y. F., Li, J. H., Song, C. Z., 2019. The Regional Tectonic Framework and some New Understandings of the Middle-Lower Yangtze River Valley Metallogenic Belt. *Acta Petrologica Sinica*, 35(12): 3579–3591. https://doi.org/10.18654/1000-0569/2019.12.01 (in Chinese with English Abstract)

Charvet, J., Lapierre, H., Yu, Y. W., 1994. Geodynamic Significance of the Mesozoic Volcanism of Southeastern China. *Journal of Southeast Asian Earth Sciences*, 9(4): 387–396. https://doi.org/10.1016/0743-9547(94)90050-7

Chu, Y., Faure, M., Lin, W., et al., 2012. Tectonics of the Middle Triassic Intracontinental Xuefengshan Belt, South China: New Insights from Structural and Chronological Constraints on the Basal Décollement Zone. *International Journal of Earth Sciences*, 101(8): 2125–2150. https://doi.org/10.1007/s00531-012-0780-5

Chu, Y., Lin, W., 2014. Phanerozoic Polyorogenic Deformation in Southern Jiuling Massif, Northern South China Block: Constraints from Structural Analysis and Geochronology. *Journal of Asian Earth Sciences*, 86: 117–130. https://doi.org/10.1016/j.jseaes.2013.05.019

Faure, M., Lin, W., Le Breton, N., 2001. Where is the North China-South China Block Boundary in Eastern China?. *Geology*, 29(2): 119–122. https://doi.org/10.1130/0091-7613(2001)029<0119:witncs>2.0.co;2

Faure, M., Marchadier, Y., Rangin, C., 1989. Pre-Eocene Synmetamorphic Structure in the Mindoro-Romblon-Palawan Area, West Philippines, and Implications for the History of Southeast Asia. *Tectonics*, 8(5): 963–979. https://doi.org/10.1029/tc008i005p00963

Ge, X. H., 1987. Nappe Structures in the Ningzhen Mountains. *Journal of Changchun Colledge of Geology*, 17(2): 143–154 (in Chinese with English Abstract)

Gilder, S. A., Leloup, P. H., Courtillot, V., et al., 1999. Tectonic Evolution of the Tancheng-Lujiang (Tan-Lu) Fault via Middle Triassic to Early Cenozoic Paleomagnetic Data. *Journal of Geophysical Research: Solid Earth*, 104(B7): 15365–15390. https://doi.org/10.1029/1999jb900123

Grimmer, J. C., Jonckheere, R., Enkelmann, E., et al., 2002. Cretaceous–Cenozoic History of the Southern Tan-Lu Fault Zone: Apatite Fission-Track and Structural Constraints from the Dabie Shan (eastern China). *Tectonophysics*, 359(3/4): 225–253. https://doi.org/10.1016/s0040-1951(02)00513-9

Hansman, R. J., Albert, R., Gerdes, A., et al., 2018. Absolute Ages of Multiple Generations of Brittle Structures by U-Pb Dating of Calcite. *Geology*, 46(3): 207–210. https://doi.org/10.1130/g39822.1

Kusky, T. M., Windley, B. F., Zhai, M. G., 2007. Tectonic Evolution of the North China Block: From Orogen to Craton to Orogen. *Geological Society, London, Special Publications*, 280(1): 1–34. https://doi.org/10.1144/sp280.1

Lapierre, H., Jahn, B. M., Charvet, J., et al., 1997. Mesozoic Felsic Arc Magmatism and Continental Olivine Tholeiites in Zhejiang Province and Their Relationship with the Tectonic Activity in Southeastern China. *Tectonophysics*, 274(4): 321–338. https://doi.org/10.1016/s0040-1951(97)00009-7

Lawrence, M. G., Kamber, B. S., 2006. The Behaviour of the Rare Earth Elements during Estuarine Mixing—Revisited. *Marine Chemistry*, 100(1/2): 147–161. https://doi.org/10.1016/j.marchem.2005.11.007

Li, H., Zhang, H., Ling, M. X., et al., 2011. Geochemical and Zircon U-Pb Study of the Huangmeijian A-Type Granite: Implications for Geological Evolution of the Lower Yangtze River Belt. *International Geology Review*, 53(5/6):

499–525. https://doi.org/10.1080/00206814.2010.496202

Li, J. H., Zhang, Y. Q., Dong, S. W., et al., 2014. Cretaceous Tectonic Evolution of South China: A Preliminary Synthesis. *Earth-Science Reviews*, 134: 98–136. https://doi.org/10.1016/j.earscirev.2014.03.008

Li, J. H., Zhao, G. C., Johnston, S. T., et al., 2017. Permo–Triassic Structural Evolution of the Shiwandashan and Youjiang Structural Belts, South China. *Journal of Structural Geology*, 100: 24–44. https://doi.org/10.1016/j.jsg.2017.05.004

Li, Q., Parrish, R. R., Horstwood, M. S. A., et al., 2014. U-Pb Dating of Cements in Mesozoic Ammonites. *Chemical Geology*, 376: 76–83. https://doi.org/10.1016/j.chemgeo.2014.03.020

Li, S. Z., Jahn, B. M., Zhao, S. J., et al., 2017. Triassic Southeastward Subduction of North China Block to South China Block: Insights from New Geological, Geophysical and Geochemical Data. *Earth-Science Reviews*, 166: 270–285. https://doi.org/10.1016/j.earscirev.2017.01.009

Li, T., Xie, G. A., Wang, G. K., et al., 2018. The Discussion About the Property and Formation Mechanism of the Dashibei Fault in Hushan, Nanjing. *Geological Journal of China Universities*, 24(6): 930–938. https://doi.org/10.16108/j.issn1006-7493.2018030 (in Chinese with English Abstract)

Li, Y., Dong, S. W., Zhang, Y. Q., et al., 2016. Episodic Mesozoic Constructional Events of Central South China: Constraints from Lines of Evidence of Superimposed Folds, Fault Kinematic Analysis, and Magma Geochronology. *International Geology Review*, 58(9): 1076–1107. https://doi.org/10.1080/00206814.2016.1146999

Li, Z.-X., Li, X.-H., 2007. Formation of the 1 300-km-Wide Intracontinental Orogen and Postorogenic Magmatic Province in Mesozoic South China: A Flat-Slab Subduction Model. *Geology*, 35(2): 179–182. https://doi.org/10.1130/g23193a.1

Li, Z.-X., Li, X.-H., Chung, S. L., et al., 2012. Magmatic Switch-on and Switch-off along the South China Continental Margin since the Permian: Transition from an Andean-Type to a Western Pacific-Type Plate Boundary. *Tectonophysics*, 532–535: 271–290. https://doi.org/10.1016/j.tecto.2012.02.011

Ling, M. X., Wang, F. Y., Ding, X., et al., 2009. Cretaceous Ridge Subduction along the Lower Yangtze River Belt, Eastern China. *Economic Geology*, 104(2): 303–321. https://doi.org/10.2113/gsecongeo.104.2.303

Liu, S. F., Zhuang, P. R., Xu, C. Y., 1992. On the Gliding—Decollement Structures Developed during Indosinian-Early Yanshannian Epoch in the Ningzhen Mountain Range. *Experimental Petroleum Geology*, 14(2): 109–115 (in Chinese with English Abstract)

Liu, S. F., Heller, P. L., Zhang, G. W., 2003. Mesozoic Basin Development and Tectonic Evolution of the Dabieshan Orogenic Belt, Central China. *Tectonics*, 22(4): 1038. https://doi.org/10.1029/2002tc001390

Lü, Q. T., Shi, D. N., Liu, Z. D., et al., 2015. Crustal Structure and Geodynamics of the Middle and Lower Reaches of Yangtze Metallogenic Belt and Neighboring Areas: Insights from Deep Seismic Reflection Profiling. *Journal of Asian Earth Sciences*, 114: 704–716. https://doi.org/10.1016/j.jseaes.2015.03.022

Lu, S. F., Zhu, X. Q., Li, X. F., 2019. Geochronology and Geochemistry of the Five Magmatic Rocks in the Ningzhen Region, China. *Acta Geochimica*, 38(2): 241–261. https://doi.org/10.1007/s11631-019-00316-2

Ludwig, K. R., 2003. User's Manual for Isoplot/Ex Version 3.00—A Geochronology Toolkit for Microsoft Excel, No. 4. Berkeley Geochronological Center, Special Publication, Berkeley CA

Nuriel, P., Rosenbaum, G., Uysal, T. I., et al., 2011. Formation of Fault-Related Calcite Precipitates and Their Implications for Dating Fault Activity in the East Anatolian and Dead Sea Fault Zones. *Geological Society*, *London*, *Special Publications*, 359(1): 229–248.

https://doi.org/10.1144/sp359.13

Nuriel, P., Weinberger, R., Kylander-Clark, A. R. C., et al., 2017. The Onset of the Dead Sea Transform Based on Calcite Age-Strain Analyses. *Geology*, 45(7): 587–590. https://doi.org/10.1130/g38903.1

Rasbury, E. T., Cole, J. M., 2009. Directly Dating Geologic Events: U-Pb Dating of Carbonates. *Reviews of Geophysics*, 47(3): RG3001. https://doi.org/10.1029/2007rg000246

Shu, L. S., Faure, M., Wang, B., et al., 2008. Late Palaeozoic–Early Mesozoic Geological Features of South China: Response to the Indosinian Collision Events in Southeast Asia. *Comptes Rendus Geoscience*, 340(2/3): 151–165. https://doi.org/10.1016/j.crte.2007.10.010

Shu, L. S., Wang, B., Cawood, P. A., et al., 2015. Early Paleozoic and Early Mesozoic Intraplate Tectonic and Magmatic Events in the Cathaysia Block, South China. *Tectonics*, 34(8): 1600–1621. https://doi.org/10.1002/2015tc003835

Shu, L. S., Zhou, X. M., Deng, P., et al., 2009. Mesozoic Tectonic Evolution of the Southeast China Block: New Insights from Basin Analysis. *Journal of Asian Earth Sciences*, 34(3): 376–391. https://doi.org/10.1016/j.jseaes.2008.06.004

Spencer, S. A. S., Kohn, B. P., Gleadow, A. J. W., et al., 2006. Fission Track Analysis and the Problematic (U-Th)/He Thermochronology of the Shandong Province, NE China—A Rifted Cratonic Margin. *Geochimica et Cosmochimica Acta*, 70(18): A606. https://doi.org/10.1016/j.gca.2006.06.1125

Su, J. B., Zhang, Y. Q., Dong, S. W., et al., 2013. Paleo-Structural Stress Field in Xuefengshan Tectonic Belt, South China. *Acta Geoscientia Sinica*, 34(6): 671–679. https://doi.org/10.3975/cagsb.2013.06.04 (in Chinese with English Abstract)

Su, J. B., Dong, S. W., Zhang, Y. Q., et al., 2014. Detrital Zircon Geochronology of Pre-Cretaceous Strata: Tectonic Implications for the Jiangnan Orogen, South China. *Geological Magazine*, 151(6): 975–995. https://doi.org/10.1017/s0016756813001003

Su, J. B., Dong, S. W., Zhang, Y. Q., et al., 2017a. Apatite Fission Track Geochronology of the Southern Hunan Province across the Shi-Hang Belt: Insights into the Cenozoic Dynamic Topography of South China. *International Geology Review*, 59(8): 981–995. https://doi.org/10.1080/00206814.2016.1240049

Su, J. B., Dong, S. W., Zhang, Y. Q., et al., 2017b. Orogeny Processes of the Western Jiangnan Orogen, South ChinaInsights from Neoproterozoic Igneous Rocks and a Deep Seismic Profile. *Journal of Geodynamics*, 103: 42–56. https://doi.org/10.1016/j.jog.2016.12.004

Su, J. B., Dong, S. W., Zhang, Y. Q., et al., 2018a. Geochronology, Geochemistry, and Tectonic Implications of Jishou Cretaceous Diabase, Western Xuefengshan Tectonic Zone in South China. *Geological Journal*, 53(3): 1186–1199. https://doi.org/10.1002/gj.2950

Su, J. B., Rao, W. B., Wang, Y. G., et al., 2018b. Detrital Zircon Geochronology of the Radial Sand Ridge System of Jiangsu Coast, East China: Implication for Sediment Provenance. *Journal of Earth Science*, 29(1): 144–154. https://doi.org/10.1007/s12583-017-0769-x

Suo, Y. H., Li, S. Z., Jin, C., et al., 2019. Eastward Tectonic Migration and Transition of the Jurassic–Cretaceous Andean-Type Continental Margin along Southeast China. *Earth-Science Reviews*, 196: 102884. https://doi.org/10.1016/j.earscirev.2019.102884

Uysal, I. T., Feng, Y. X., Zhao, J. X., et al., 2007a. U-Series Dating and Geochemical Tracing of Late Quaternary Travertine in Co-Seismic Fissures. *Earth and Planetary Science Letters*, 257(3/4): 450–462. https://doi.org/10.1016/j.epsl.2007.03.004

Uysal, I. T., Zhao, J. X., Golding, S. D., et al., 2007b. Sm-Nd Dating and

Rare-Earth Element Tracing of Calcite: Implications for Fluid-Flow Events in the Bowen Basin, Australia. *Chemical Geology*, 238(1/2): 63–71. https://doi.org/10.1016/j.chemgeo.2006.10.014

Wang, Y. J., Zhang, Y. H., Fan, W. M., et al., 2005. Structural Signatures and ^{40}Ar/^{39}Ar Geochronology of the Indosinian Xuefengshan Tectonic Belt, South China Block. *Journal of Structural Geology*, 27(6): 985–998. https://doi.org/10.1016/j.jsg.2005.04.004

Xu, J. F., Shinjo, R., Defant, M. J., et al., 2002. Origin of Mesozoic Adakitic Intrusive Rocks in the Ningzhen Area of East China: Partial Melting of Delaminated Lower Continental Crust?. *Geology*, 30(12): 1111–1114. https://doi.org/10.1130/0091-7613(2002)030<1111:oomair>2.0.co;2

Xu, Y. M., Jiang, S. Y., Zhu, Z. Y., et al., 2014. Petrogenesis of Late Mesozoic Granitoids and Coeval Mafic Rocks from the Jiurui District in the Middle–Lower Yangtze Metallogenic Belt of Eastern China: Geochemical and Sr-Nd-Pb-Hf Isotopic Evidence. *Lithos*, 190/191: 467–484. https://doi.org/10.1016/j.lithos.2013.12.022

Xue, H. M., 2019. Late Mesozoic Adakitic Intrusive Rocks in Ningzhen District, Lower Yangtze River Reaches: Ages, Geochemical and Genesis. *Acta Geologica Sinica*, 93(1): 147–169. https://doi.org/10.19762/j.cnki.dizhixuebao.2019008 (in Chinese with English Abstract)

Zhang, Y. Q., Dong, S. W., Shi, W., 2003. Cretaceous Deformation History of the Middle Tan-Lu Fault Zone in Shandong Province, Eastern China. *Tectonophysics*, 363(3/4): 243–258. https://doi.org/10.1016/s0040-1951(03)00039-8

Zhang, Z. W., Shu, Q., Yang, X. Y., et al., 2019. Review on the Tectonic Terranes Associated with Metallogenic Zones in Southeast Asia. *Journal of Earth Science*, 30(1): 1–19. https://doi.org/10.1007/s12583-019-0858-0

Zhou, X. M., Sun, T., Shen, W. Z., et al., 2006. Petrogenesis of Mesozoic Granitoids and Volcanic Rocks in South China: A Response to Tectonic Evolution. *Episodes*, 29(1): 26–33. https://doi.org/10.18814/epiiugs/2006/v29i1/004

Zhu, G., Wang, D. X., Liu, G. S., et al., 2004. Evolution of the Tan-Lu Fault Zone and Its Responses to Plate Movements in West Pacific Basin. *Chinese Journal of Geology*, 39(1): 36–49 (in Chinese with English Abstract)

Zhu, G., Xu, J. W., Liu, G. S., et al., 1998. Tectonic Control on Development of the Foreland Basin along the Yangtze River in the Lower Yangtze River Region. *Geological Review*, 44(2): 120–129. https://doi.org/10.16509/j.georeview.1998.02.002 (in Chinese with English Abstract)

Zhu, G., Liu, C., Gu, C. C., et al., 2018. Oceanic Plate Subduction History in the Western Pacific Ocean: Constraint from Late Mesozoic Evolution of the Tan-Lu Fault Zone. *Science China Earth Sciences*, 61(4): 386–405. https://doi.org/10.1007/s11430-017-9136-4